

Instabilities of Galactic Disks in the Presence of Star Formation

Adi Nusser^{1,2}

¹*Physics Department and the Asher Space Research Institute, Technion, Haifa 32000, Israel*

²*Astrophysics, Oxford University, Keble Rd, Oxford OX1 3RK, UK*

25 August 2018

ABSTRACT

We discuss the stability of galactic disks in which the energy of interstellar clouds is gained in encounters with expanding supernova remnants and lost in inelastic collisions. Energy gain and loss processes introduce a phase difference between the pressure and density perturbations, making disks unstable on small scales for several recipes of star formation. This is in contrast to the standard stability analysis in which small scale perturbations are stabilized by pressure. In the limit of small scales the dispersion relation for the growth rate reduces to that of thermal instabilities in a fluid without gravity. If instabilities lead to star formation, then our results imply a secondary mode of star formation which operates on small scales and feeds on the existence of a primary mode on intermediate scales. This may be interpreted as a positive feedback. Further, the standard stability criterion on intermediate scales is significantly modified.

Key words: galaxies: structure -instabilities - stars: formation

1 INTRODUCTION

Instability and star formation in galactic disks are intimately linked. The observational support for that is the significant decline of star formation activity in regions with relatively low gas mass surface density, as expected from various stability analyses (e.g. Martin & Kennicutt 2001). Theoretically, the collapse of cold gas provides ripe conditions for the appearance of molecular clouds and, subsequently, star formation. (e.g. Spitzer 1968, Quirk 1972).

On large scales (of the order of the size of the disk) perturbations are stabilized by rotation. Disks are also stable on small scales if the pressure, P , and density, ρ , are related by $P \propto \rho^\gamma$, where γ is a constant. On intermediate scales, neither rotation nor pressure can stop gravity from amplifying the perturbations if the surface density is above a critical value. The first detailed stability calculations for single fluid disks have been done in two classic papers by Toomre (1964) and Goldreich & Lynden-Bell (1965). Similar type of analysis has been generalized to the more realistic case of disks containing stellar and gaseous components (Jog & Solomon 1984, Rafikov 2001, Griv, Gedalin & Yuan 2002). Viscous disks have also been considered and found to be always unstable, with small scale perturbations growing at a low rate that is set by the viscosity (Gammie 1996). These

studies have assumed that the perturbation in the pressure is proportional that in the density.

Here we consider the instability of the interstellar cloud component of the disk, when it is subject to local energy gain and loss processes. Clouds gain energy in encounters with expanding supernova (SN) remnants, and lose energy in inelastic collisions among each other (McKee & Ostriker 1977, hereafter MO77). Both of these processes depend, in general, on the local surface density and velocity dispersion of the clouds. The star formation rate is enhanced above the global average in a region with a positive density fluctuation, resulting in a local increase of the velocity dispersion. A perturbation in the velocity dispersion changes the energy loss rate and may also affect the star formation rate. We perform detailed stability analysis under the assumption that the cloud component be treated as a hydrodynamical fluid over sufficiently large length and temporal scales. The treatment here leads to a significant modification of the standard stability criteria. We get instabilities on much smaller scales than what is inferred from the standard analysis. In several important cases, instabilities extend down to the scale where the fluid treatment becomes invalid.

The paper is organized as follows. The equations are derived and expanded in Laplace transforms in §2. Stability analysis is presented in §3. This section includes a classification of stable and unstable modes by means of Nyquist

arXiv:astro-ph/0503042v2 26 May 2005

diagrams, a discussion of a few limiting cases, and a treatment of instabilities with specific form for the energy gain and loss rates. The validity of our approach is assessed in §5. A summary and discussion of the results are presented in §6.

2 THE EQUATIONS

We write the equations governing the evolution of perturbations in a thin gaseous disk. The gas represents interstellar clouds which, for simplicity, are assumed to have isotropic velocity dispersion. We assume that the gas has an ideal equation of state which after integration over the height of the disk yields

$$p = (\gamma - 1)\mu \varepsilon \quad (1)$$

to relate the “two-dimensional” pressure, p , to the mass surface density, μ , and the “random” kinetic energy per unit mass, $\varepsilon = V_{\text{rms}}^2/2$, where V_{rms} is the three dimensional velocity dispersion of the clouds, and $\gamma > 1$. We will also refer to ε as internal energy. The adiabatic index γ relates the projected quantities and, therefore, is in general different from the physical three dimensional index, Γ . The relation between γ and Γ depends on the structure of the disk. For a self gravitating disk $\gamma = 3 - 2/\Gamma = 9/5$ for $\Gamma = 5/3$ (e.g. Gammie 2001). The difference between the two indices has little effect in our applications and so we present numerical results only for $\gamma = 5/3$. We write energy conservation in the following form,

$$\frac{d\varepsilon}{dt} = \frac{p}{\mu^2} \frac{d\mu}{dt} + G - L, \quad (2)$$

where $G(\mu, \varepsilon)$ and $L(\mu, \varepsilon)$ are, respectively, the energy gain and loss rates per unit mass, assumed to be explicit functions of μ and ε alone. In the meantime we will study some general features of the stability of the system without referring to specific forms for G and L .

Let the disk be in a steady state in which the disk is axisymmetric, gravity is balanced by rotation, and energy gain is balanced by energy loss, i.e. $G = L$. This steady state is characterized by the rotational speed, $\Omega(r)$, the gas mass surface density, $\mu_0(r)$, and the internal energy per unit mass, $\varepsilon_0(r)$, as functions of the distance from the center of the disk, r . We are interested in the linear response of the system to small perturbations from this steady state. For simplicity we consider only radial perturbations as the complication introduced by non-axisymmetric perturbations does not hide any additional relevant physical effects. Let u , v , $\mu^{(1)}$, $\varepsilon^{(1)}$, $p^{(1)}$, and $\phi^{(1)}$ be, respectively, the perturbations in the radial velocity, the transverse velocity, the surface density, the internal energy, the pressure, and the gravitational potential field. The first order equations governing the evolution

of these perturbations are

$$p^{(1)} = (\gamma - 1)\mu_0 \varepsilon^{(1)} + (\gamma - 1)\varepsilon_0 \mu^{(1)}, \quad (3)$$

$$\partial_t \varepsilon^{(1)} = \frac{p_0}{\mu_0^2} \partial_t \mu^{(1)} + C_\mu \mu^{(1)} + C_\varepsilon \varepsilon^{(1)}, \quad (4)$$

$$\partial_t u - 2\Omega(r)v + \partial_r p^{(1)}/\mu_0(r) + \partial_r \phi^{(1)}|_{z=0} = 0, \quad (5)$$

$$\partial_t v - 2B(r)u = 0, \quad (6)$$

$$\partial_t \mu^{(1)} + \partial_r [r\mu_0(r)u] = 0, \quad (7)$$

$$\partial_r (r\partial_r \phi^{(1)})/r + \partial_z^2 \phi^{(1)} = 4\pi G\mu_1 \delta^D(z), \quad (8)$$

where $p_0 = (\gamma - 1)\varepsilon_0\mu_0$, and

$$C_\mu = \frac{\partial(G - L)}{\partial\mu}|_{\mu_0, \varepsilon_0} \quad \text{and} \quad C_\varepsilon = \frac{\partial(G - L)}{\partial\varepsilon}|_{\mu_0, \varepsilon_0}. \quad (9)$$

The first two of these equations are obtained by linearization of equations (1) and(2), respectively. The equations (5) and (6) are the radial and transverse linear versions of the Euler equations. Mass conservation is represented by (7) and the Poisson equation by (8). We expand the perturbations in Fourier modes, $\exp(i\mathbf{k} \cdot \mathbf{r})$. Considering only modes satisfying $kr \gg 1$, the linear equations lead to,

$$\dot{\varepsilon}_1 = \frac{p_0}{\mu_0^2} \dot{\mu}_1 + C_\mu \mu_1 + C_\varepsilon \varepsilon_1 \quad (10)$$

$$\ddot{\mu}_1 + [\kappa^2 - 2\pi G\mu_0 k + (\gamma - 1)\varepsilon_0 k^2] \mu_1 + (\gamma - 1)\mu_0 k^2 \varepsilon_1 = 0, \quad (11)$$

where μ_1 is defined by $\mu^{(1)}(r, t) = \mu_1(t) \exp(i\mathbf{k} \cdot \mathbf{r})$ and similarly for ε_1 , and $\kappa = 2\Omega[1 + (d \ln \Omega / d \ln r) / 2]^{1/2}$ is the epicyclic frequency. In deriving these equations, the relation $\partial_r \phi^{(1)}|_{z=0} = i2\pi G\mu_1 \exp(i\mathbf{k} \cdot \mathbf{r})$ has been used (Toomre 1964).

The differential equations (10) and (11) are linear with constant coefficients and they can be solved by means of Laplace transformation (see Appendix A). By taking the Laplace transform of (10) and (11) we get

$$s\mathcal{E} - \varepsilon_1(0) = (\gamma - 1)\frac{\varepsilon_0}{\mu_0}(s\mathcal{M} - \mu_1(0)) + C_\mu \mathcal{M} + C_\varepsilon \mathcal{E}, \quad (12)$$

$$s^2 \mathcal{M} - s\mu_1(0) - \dot{\mu}_1(0) + [\kappa^2 - 2\pi G\mu_0 k + (\gamma - 1)\varepsilon_0 k^2] \mathcal{M} + (\gamma - 1)\mu_0 k^2 \mathcal{E} = 0, \quad (13)$$

where $\mathcal{M}(s)$ and $\mathcal{E}(s)$ are the Laplace transforms of $\mu_1(t)$ and $\varepsilon_1(t)$, respectively, and $\mu_1(0)$, $\dot{\mu}_1(0)$, and $\varepsilon_1(0)$ represent the initial conditions given at $t = 0$. Solving for \mathcal{M} yields,

$$B(s)\mathcal{M}(s) = (s - C_\varepsilon)[s\mu_1(0) + \dot{\mu}_1(0)] \quad (14)$$

$$+ (\gamma - 1)\mu_0 k^2 [\varepsilon_1(0) - (\gamma - 1)\frac{\varepsilon_0}{\mu_0} \mu_1(0)], \quad (15)$$

where

$$B(s) = s^3 - s^2 C_\varepsilon + s\omega_0^2 - C_\varepsilon \omega_1^2, \quad (16)$$

with

$$\omega_0^2(k) = \kappa^2 - 2\pi G\mu_0 k + \gamma(\gamma - 1)\varepsilon_0 k^2, \quad (17)$$

$$\omega_1^2(k) = \omega_0^2 - (\gamma - 1)\varepsilon_0 k^2 \left(\frac{\mu_0 C_\mu}{\varepsilon_0 C_\varepsilon} + \gamma - 1 \right). \quad (18)$$

The third order polynomial $B(s)$ has at most three distinct roots, s_j ($j = 1, 2, 3$). Since $\mathcal{M}(s) \propto 1/B(s)$ then according to the theory of Laplace transforms (see Appendix A) $\mu_1(t)$ is a linear combination of $\exp(s_j t)$. Therefore, an unstable (growing) mode corresponds to a root with a positive real part.

In the limit of small scales, i.e. large k , the terms proportional to k^2 are dominant in (17) and (18). This means that the effects of rotation and self-gravity are negligible. In this limit, the characteristic equation $B(s) = 0$, reduces to the dispersion relation derived by Field (1965) for the growth rate of thermal instabilities (see Eq. 15 in Field 1965, without the thermal conduction term).

3 STABILITY ANALYSIS

Our task is to establish the relevant time scales for the evolution of the perturbations and classify the stable and unstable modes. The three time scales corresponding to the roots s_j of $B(s)$ must be reflected in C_ε , ω_0 and ω_1 . We will find that C_ε is negative for the specific forms of G and L we use below. The dependence on C_ε can be scaled out by working with the variables $\tilde{s} = s/(-C_\varepsilon)$, $\tilde{\omega}_0 = \omega_0/(-C_\varepsilon)$ and $\tilde{\omega}_1 = \omega_1/(-C_\varepsilon)$. If \tilde{s}_j ($j = 1, 2, 3$) solves

$$\tilde{s}^3 + \tilde{s}^2 + \tilde{s}\tilde{\omega}_0^2 + \tilde{\omega}_1^2 = 0, \quad (19)$$

then $s_j = -C_\varepsilon \tilde{s}_j$. Therefore, the stability of a mode with a wave-number k , depends only on $\omega_0^2(k)$ and $\omega_1^2(k)$. The time scales, however, may depend nontrivially on C_ε .

The roots of $B(s)$ can either be all real (with zero imaginary parts) or one real and two conjugate complex roots (i.e. having the same real part). The sum of the roots is $s_1 + s_2 + s_3 = C_\varepsilon < 0$ and therefore at least one of them must have a negative real part, meaning that there is always a decaying mode. The question of the existence of unstable modes for any combination of ω_0^2 and ω_1^2 can be addressed by Nyquist diagrams (Nyquist 1932, see also Appendix B). These diagrams provide a simple way to determine the number of roots lying to right of the imaginary axis (i.e. roots with positive real parts) without having to solve the third order equation $B(s) = 0$. The outcome of this analysis is as follows (we refer only to roots lying to the right of the imaginary axis),

- (i) $\omega_0^2 > \omega_1^2 > 0$: no roots
- (ii) $\omega_1^2 > \omega_0^2 > 0$: 2 complex roots
- (iii) $\omega_0^2 > 0, \omega_1^2 < 0$: 1 root
- (iv) $\omega_0^2 < 0, \omega_1^2 < 0$: 1 root
- (v) $\omega_0^2 < 0, \omega_1^2 > 0$: 2 root (either 2 real or 2 complex conjugates)

Therefore, the disk is stable only for $\omega_0^2 > \omega_1^2 > 0$.

3.1 limiting cases

Nyquist diagrams do not contain any information on the instability time scales. Those could be obtained by numer-

ically finding the roots of $B(s)$. Here we discuss a few important limiting cases that can be studied analytically. Let $\Delta\tilde{\omega}^2 = \tilde{\omega}_1^2 - \tilde{\omega}_0^2$. First consider the limit, $|\Delta\tilde{\omega}^2| \ll |\tilde{\omega}_0^2|$ in which the roots differ by small amount from the values $\tilde{s} = -1$ and $\tilde{s} = \pm\sqrt{-\tilde{\omega}^2}$ which solve (19) with $\Delta\tilde{\omega}^2 = 0$. In this case,

$$\begin{aligned} s_1 &= -|C_\varepsilon| \frac{1 + (\omega_1/C_\varepsilon)^2}{1 + (\omega_0/C_\varepsilon)^2}, \\ s_{2,3} &= |C_\varepsilon| \frac{\pm|C_\varepsilon| \sqrt{-\omega_0^2 + \omega_0^2} \frac{\omega_1^2 - \omega_0^2}{2\omega_0^2} \pm \sqrt{-\omega_0^2}}{C_\varepsilon^2 + \omega_0^2}. \end{aligned} \quad (20)$$

Note that these expressions involve C_ε in a complicated way. For $\omega_1^2 > \omega_0^2 > 0$ the system is unstable, in accordance with the Nyquist analysis, with a growth time scale of $[\text{Re}(s_2)]^{-1} = [(1/2)C_\varepsilon(\omega_1^2 - \omega_0^2)/(C_\varepsilon^2 + \omega_0^2)]^{-1}$. For $\omega_0^2 > \omega_1^2 > 0$ there are no unstable modes.

The second and more important limit is when $\tilde{\omega}_0^2 \gg 1$ and $\Delta\tilde{\omega}^2 = \mathcal{O}(\omega_0^2)$. This holds for small scale perturbations since for sufficiently large k the leading term in ω_0^2 is the one involving k^2 (see eq. 17). The roots of $B(s)$ are approximated by,

$$s_1 = -|C_\varepsilon| \frac{\omega_1^2}{\omega_0^2} \quad \text{and} \quad s_{2,3} = |C_\varepsilon| \frac{\omega_1^2 - \omega_0^2}{2\omega_0^2} \pm i\omega_0. \quad (21)$$

For $\omega_1^2 > \omega_0^2$ the root s_1 represent a decaying mode, while the conjugate roots s_2 and s_3 correspond to sound waves that grow at a rate proportional to $|C_\varepsilon|$ and oscillate with frequency of $\omega_0/2\pi$. The origin of the growth is heating occurring during the compression the waves (c.f. Field 1965). In terms of C_μ and C_ε the condition, $\omega_1^2 > \omega_0^2$, for the appearance of growing sound waves reads,

$$\frac{\mu_0 C_\mu}{\varepsilon_0 C_\varepsilon} + \gamma - 1 < 0,$$

which is similar to the condition in Eq.24 of Field 1965. For $\omega_0^2 > \omega_1^2 > 0$ all modes are decaying with s_2 and s_3 representing overstable (oscillating) modes. For $\omega_0^2 > 0$ but $\omega_1^2 < 0$ the mode s_1 is growing without oscillations and s_2 and s_3 are overstable modes. The mode described by s_1 corresponds to growth by condensation under nearly constant pressure conditions as described by Field (1965). It can result from an enhanced cooling efficiency as the density is increased. The condition $\omega_1^2 < 0$ holds for

$$1 - \frac{\mu_0 C_\mu}{\varepsilon_0 C_\varepsilon} < 0. \quad (22)$$

This is equivalent to the condition for a condensation mode as given by Eq.23 of Field 1965.

3.2 Numerical solutions

To better visualize the time dependence of perturbations we plot in figure (1) the functions $\mu_1(t)$ and $\varepsilon_1(t)$ for $\omega_1^2 < 0$ (top panel), $\omega_0^2 > \omega_1^2 > 0$ (middle) and $\omega_1^2 > \omega_0^2$ (bottom). The figure shows only cases with $\omega_0^2 > 0$ which is always true for sufficiently large k . These curves have been obtained by numerical integration of the following dimensionless form of

(10) and (11),

$$\tilde{\mu}_1'' + \left[1 - \frac{2}{Q_0} \tilde{k} + \tilde{k}^2 \right] \tilde{\mu}_1 + \tilde{k}^2 \tilde{\varepsilon}_1 = 0, \quad (23)$$

$$\tilde{\varepsilon}_1' = (\gamma - 1) \tilde{\mu}_1' + \tilde{C}_\mu \tilde{\mu}_1 + \tilde{C}_\varepsilon \tilde{\varepsilon}_1, \quad (24)$$

where the prime symbol denotes differential with respect to the variable $t\kappa$, $k_0 = \pi G \mu_0 / ((\gamma - 1) \varepsilon_0 Q_0)$, $\tilde{k} = k/k_0$, $Q_0 = \kappa [(\gamma - 1) \varepsilon_0]^{1/2} / (\pi G \mu_0)$, $\tilde{\varepsilon}_1 = \varepsilon_1 / \varepsilon_0$, $\tilde{\mu}_1 = \mu_1 / \mu_0$, $\tilde{C}_\mu = \mu_0 C_\mu / (\varepsilon_0 / \kappa)$, and $\tilde{C}_\varepsilon = C_\varepsilon / \kappa$. All solutions are for $\tilde{C}_\varepsilon = -1$, $\tilde{k} = 5$, $Q_0 = 1$, and $\gamma = 5/3$. The solutions in the top, middle and bottom panels correspond to $\tilde{C}_\mu = -1.3$, 0, and 2, respectively. The initial conditions of all solutions are $\tilde{\mu}_1(0) = \tilde{\varepsilon}_1(0) = 1$ and $\tilde{\mu}_1'(0) = 0$. The behavior of the solutions is in agreement with Nyquist diagrams and the limiting cases. For $\omega_1^2 > \omega_0^2 > 0$ (bottom panel), the solution is oscillatory with a growing envelope. These growing sound waves arise because of the slight heating during compression. The case $\omega_0^2 > \omega_1^2 > 0$ is overstable. Note that the derivative of $\tilde{\varepsilon}_1$ at $\tau = 0$ is positive although the dotted curve may appear as declining at $\tau = 0$. The phase difference between the dotted and solid curves, however, becomes more evident as τ increases.

For $\omega_1 < 0$ and $\omega_0^2 > 0$ the solution is unstable without oscillations. This mode is driven by thermal instability of a condensation mode (Field 1965). Note the phase difference between μ_1 and ε_1 . This phase difference is the drive behind the instabilities shown in the top and bottom panels.

4 STABILITY WITH SPECIFIC FORMS OF G AND L

A key parameter is the ratio $\mu_0 C_\mu / \varepsilon_0 C_\varepsilon$ which determines the difference between ω_1^2 and ω_0^2 (see Eq.18). This ratio depends on the specific forms chosen to describe the energy gain and loss functions.

The function $L(\mu, \varepsilon)$ represents energy dissipation per units mass, via inelastic cloud collisions. Hereafter we adopt the following form (MO77, Efsthathiou 2002),

$$L = \eta_L \mu^2 \varepsilon^{1/2}. \quad (25)$$

The energy gain function, G , is directly proportional to the star formation rate (MO77). We work with two distinct choices, the first is a Schmidt-Kennicutt (e.g. Kennicutt 1989) form and the second assumes that the star formation rate depends explicitly on the Toomre parameter which governs instabilities on intermediate scales.

4.1 Stability with a Schmidt-Kennicutt star formation law

Here we write the energy gain function as,

$$G = \eta_G \mu^n, \quad (26)$$

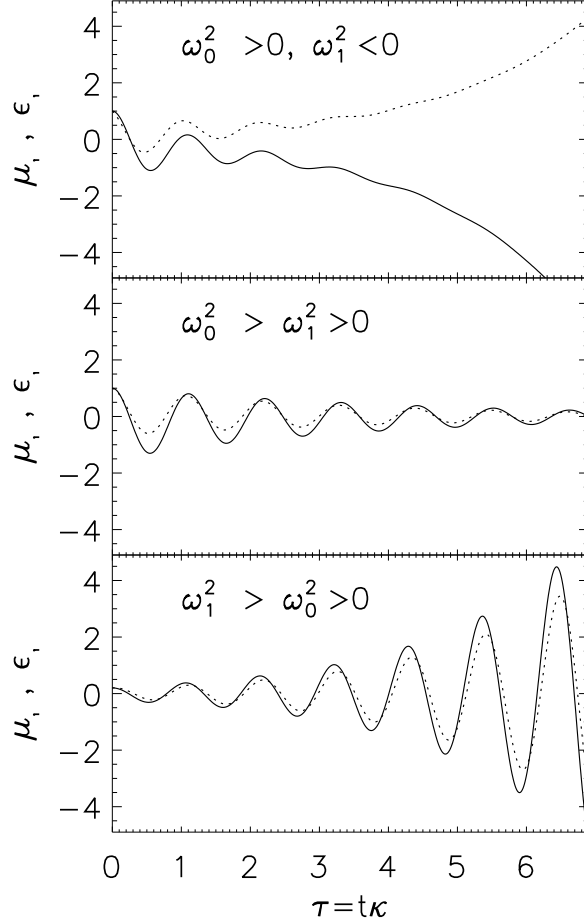


Figure 1. The time evolution of the perturbations in the surface density (solid line) and internal energy (dotted) in arbitrary units. The curves have been obtained by direct numerical integration of the equations of motion.

where η_G is a numerical factor having the appropriate units. Equating this G with L given by (25) gives,

$$C_\mu = (n - 2) \eta_G \mu_0^{n-1} \quad \text{and} \quad C_\varepsilon = -\frac{1}{2} \frac{\eta_L}{\eta_G} \mu_0^{4-n}. \quad (27)$$

Therefore, using (18),

$$\omega_1^2 = \omega_0^2 + (\gamma - 1)(2n - 3 - \gamma) \varepsilon_0 k^2. \quad (28)$$

Of particular interest is the small scale behavior. For sufficiently large k we write $\omega_0^2 \approx \gamma(\gamma - 1) \varepsilon_0 k^2$. Therefore, for $n < 3/2$, we have $\omega_1^2 < 0$, while for $n > (3 + \gamma)/2$, we have $\omega_1^2 > \omega_0^2$. The disk is unstable in these two cases. But the nature of the instability is different: the former is described by a single non-oscillatory mode, while the latter has two growing oscillatory modes (see fig. 1 and the discussion of Nyquist diagrams at the end of §3).

We plot in figure (2) the real parts of the roots as a function of the wave number k for $n = 1.5$ (top panel) and $n = 2$ (bottom). The dashed line is the instability growth rate according to the standard analysis à la Toomre (1964). This is given by $\sqrt{-\omega_0^2}$ for $\omega_0^2 < 0$, and zero otherwise. A value of $\gamma = 5/3$ is used and κ , μ_0 and ε_0 have been tuned so that the maximum of the dashed curve is consistent with the growth rate inferred from the lower curve of Fig.1a of

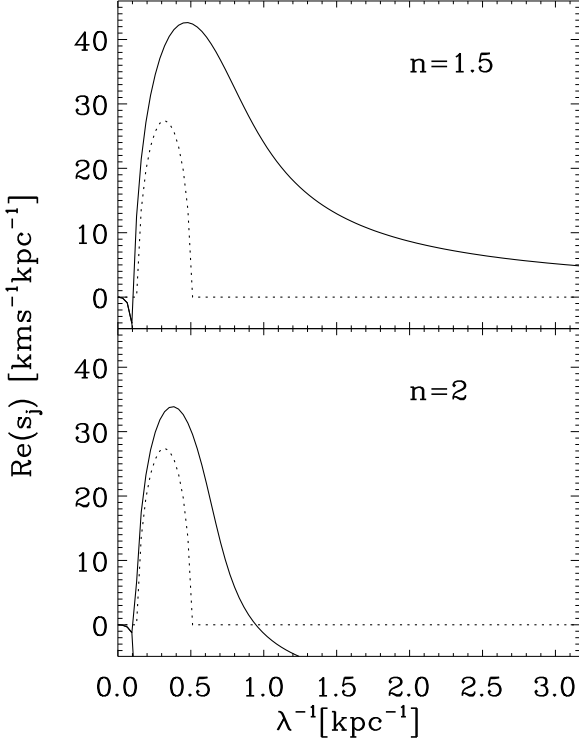


Figure 2. The growth rate of the unstable modes as function of the scale $\lambda^{-1} = k/2\pi$. The top and bottom panels show results for two values of the power index of the star formation rate, n . The solid line is the real part of the root of $B(s)$. The dashed line is the growth rate estimated as $(-\omega_0^2)^{1/2}$ for $\omega_0^2 < 0$ and zero otherwise. The values of the various parameters were chosen such that the minimum of ω_0^2 matches the value given in Jog & Solomon (1984).

Jog & Solomon (1984). We use $|C_\varepsilon| = 20 \text{ km s}^{-1} \text{ kpc}^{-1}$, corresponding to a time scale of $5 \times 10^7 \text{ yr}$ (MO77). The solid line shows the positive real parts of the roots. According to the solid curve the system with $n = 1.5$ remains unstable on small scales, albeit with a longer time scale than the instabilities at intermediate scales. For $n = 2$ the instability extends to smaller scales than what would be inferred from the standard analysis (dashed line).

4.2 Q dependent star formation rate

Assume now that the star formation rate depends on the time scale defined by standard stability analysis (e.g. Toomre 1964). We work with a gain function of the form (e.g. Wang & Silk 93, Elmegreen 1999),

$$G = \eta_G \kappa \mu F(Q) \quad (29)$$

where

$$Q = \frac{\kappa \varepsilon^{1/2}}{\pi G \mu} \quad \text{and} \quad F = \frac{(1 - Q^2)^{1/2}}{Q}. \quad (30)$$

Note that the meaning of η_G is different from (26); the same symbol is used only for the sake of brevity. Energy balance ($G=L$) at $\mu = \mu_0$ and $\varepsilon = \varepsilon_0$ yields

$$F(Q) = Q/K, \quad (31)$$

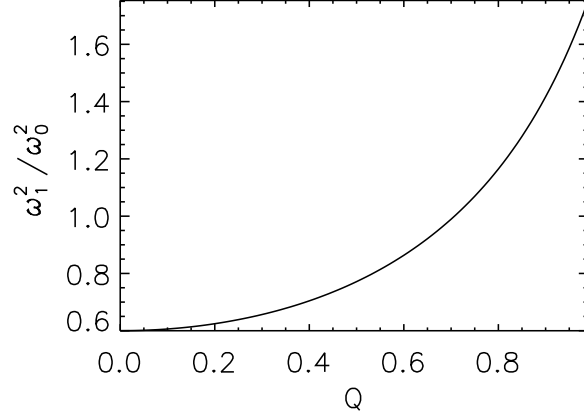


Figure 3. The ratio ω_1^2/ω_0^2 as a function of the Toomre parameter for the Wang & Silk star formation rate. The ratio is computed in the limit $k \rightarrow \infty$. The system is unstable when the ratio exceeds unity.

where $1/K = (\frac{\eta_L}{\eta_G})(\frac{2\pi G}{\kappa^2})\mu_0^2$. This relation gives,

$$Q^2 = -\frac{K^2}{2} + \frac{K^2}{2} \left(1 + \frac{4}{K^2}\right)^{1/2}. \quad (32)$$

For $K \ll 1$ and $K \gg 1$ we have $Q = K^{1/2}$ and $Q = 1$, respectively. The first order variation of $(G - L)$ is

$$\delta G - \delta L = \eta_G \kappa \left[F \mu_1 + \mu \frac{dF}{dQ} \frac{\partial Q}{\partial \mu} \mu_1 + \mu \frac{dF}{dQ} \frac{\partial Q}{\partial e} \varepsilon_1 \right] \quad (33)$$

$$-2\eta_L \mu e^{1/2} \mu_1 - \frac{1}{2} \eta_L \mu^2 e^{-1/2} \varepsilon_1 \quad (34)$$

Comparing this expression with the definitions of C_μ and C_ε (see Eq. 9) and using $\partial Q/\partial \mu = -Q/\mu$, $\partial Q/\partial e = Q/(2e)$ and $\varepsilon^{1/2} = 2\pi G \mu Q/\kappa$ we get,

$$C_\mu = -\eta_G \kappa \left(1 + \frac{d \ln F}{d \ln Q}\right) F, \quad (35)$$

$$C_\varepsilon = -\eta_G \kappa \frac{\mu_0}{2\varepsilon_0} \left(1 - \frac{d \ln F}{d \ln Q}\right) F. \quad (36)$$

Since $d \ln F/d \ln Q < 0$, the coefficient C_ε is negative. By evaluating the logarithmic derivative in terms of Q we find, $\mu C_\mu/\varepsilon C_\varepsilon = 2Q^2/(Q^2 - 2)$, and

$$\omega_1^2 = \omega_0^2 - (\gamma - 1)\varepsilon_0 k^2 \left(\gamma - 1 + \frac{2Q^2}{Q^2 - 2} \right). \quad (37)$$

For $Q^2 > 2(\gamma - 1)/(\gamma + 1)$, we have $\omega_1^2 > \omega_0^2$, yielding unstable modes even on small scales. For lower q , the system is stable on small scales but, as in the case with $n = 2$ of the previous subsection, unstable modes extend to scales smaller than in the standard analysis. The ratio ω_1^2/ω_0^2 as a function of Q is plotted in figure (3), in the limit of very large k . A value of $\gamma = 5/3$ is used in this figure.

5 VALIDITY OF THE APPROACH

The treatment of the clouds as a hydrodynamical fluid is valid over scales larger than the mean free path, l_{fp} ,

for cloud-cloud collisions. In the solar neighborhood $l_{\text{fp}} \approx 100$ pc for the cold neutral cores and about 10 pc if the warm envelopes are included (MO77). Although the warm envelopes should contribute to the collisions, we take $l_{\text{fp}} \approx 100$ pc as an upper limit.

Further, there are two time scale to be considered. First, there is the mean time between collisions, $t_{\text{coll}} = l_{\text{fp}}/V_{\text{rms}} \approx 3 \times 10^6$ yr for $V_{\text{rms}} = 10 \text{ kms}^{-1}$. Second, there is the mean time, t_{reheat} , between two successive ‘‘heating’’ events of a cloud. This comes about because we assume that multiple encounters with with expanding SN remnants eventually amount to an increase in random kinetic energy rather than bulk motions. According to Cox & Smith (1974) $t_{\text{reheat}} \sim 10^6 - 10^7$ yr.

There is also the length scale over which the velocity dispersion can equilibrate in a time $t = \max(t_{\text{reheat}}, t_{\text{coll}})$. This scale arises from the finite mean free path of the clouds (see also Gammie 1996) and is similar to the usual heat conduction (e.g. Zel’dovich & Raizer 2002). We estimate this scale as $(tV_{\text{rms}}l_{\text{fp}})^{1/2}$. Taking $t = t_{\text{coll}}$ yields a scale of $(t_{\text{coll}}V_{\text{rms}}l_{\text{fp}})^{1/2} = l_{\text{fp}}$.

Therefore, for an environment like the solar neighborhood, our approach is valid over scales larger than a hundred parsecs. The scale is sufficiently small that our treatment remains interesting. For example, this scale is smaller than the scale of unstable modes found by means of standard stability analysis (e.g. Toomre 1964, Jog & Solomon 1984).

Finally, there is a continuous process of cloud destruction and production. We assume that this process is rapid and always produces a fixed spectrum for the cloud size distribution.

6 SUMMARY AND DISCUSSION

We have considered the instability of gaseous disks subject to local energy gain and loss processes in the presence of star formation. The gas represents interstellar clouds and the energy is gained in repeated encounters of the clouds with expanding SN remnants and is lost in inelastic cloud-cloud collisions. These energy exchange processes introduce a phase difference between the density and pressure perturbations. In several interesting situations this phase difference causes the pressure to amplify the density perturbation. For a star formation rate proportional to μ^n the instabilities extend to much smaller scales than what is inferred from standard stability analyses à la Toomre (1964) and Goldreich & Lynden-Bell (1965).

The small scale instabilities may be responsible for triggering further star formation. Therefore, there may be two modes of star formation, a primary mode on intermediate scales and a secondary mode operating on small scales at a rate that is determined by the coefficient C_ϵ (see Eq. 9). This can be interpreted as positive feedback in which the intermediate scale mode is driving star formation on smaller scales through the development of instabilities. It is unclear what gain function one should use in (2). A fully self-consistent stability analysis should incorporate the energy gain result-

ing from the star formation mode that is induced by the instabilities. This complicates the problem substantially since the form of the gain function in this case must be derived from the stability analysis self-consistently. Nevertheless, we have found that small scale instabilities develop at some level for most generic forms of the gain function. We do not expect a full self-consistent treatment to change our conclusions significantly.

We have not included the coupling of gas to the stellar component. This could easily be done, but does not affect the main conclusions of the present work. Including the stellar component would tend to destabilize small scale modes even further (Jog & Solomon 1984).

ACKNOWLEDGMENT

The author thanks Joe Silk for stimulating discussions, and an anonymous referee for pointing out an error in a previous version of the paper and for several useful comments and clarifications.

REFERENCES

- Cox D.P., Smith B.W., 1974, ApJ, 189, L105
 Efstathiou G., 2000, MNRAS, 317, 697
 Elmegreen B.G., 1999, Proceedings of Star Formation 1999, Editor: Nakamoto T.
 Nyquist H., 1932, Bell. Syst. Technol. J., 11, 126, 139, 1217
 Field G., 1965, ApJ, 142, 531
 Gammie C.F., 1996, ApJ, 462, 725
 Gammie C.F., 2001, ApJ, 553, 174
 Goldreich P., Lynden-Bell D., 1965, MNRAS, 130, 97
 Griv E., Gedalin M., Yuan C., 2002, A&A, 383, 338
 Hunter D.A., Elmegreen B.G., Baker A.L., 1998, ApJ, 493, 595
 Jog C.J., Solomon P.M., 1984, ApJ, 276, 114
 Kennicutt R., 1989, ApJ, 344, 685
 Martin C.L., Kennicutt R.C., 2001, ApJ, 555, 301
 McKee C.F., Ostriker J.P., 1977, ApJ, 218, 148
 Quirk W.J., 1972, ApJ, 176, L9
 Rafikov R.R., 2001, MNRAS, 323, 445
 Spitzer L., 1968, Diffuse Matter in Space (New York: Wiley)
 Toomre A., 1964, ApJ, 139, 1217
 Wang B., Silk J., 1993, ApJ, 427, 759
 Zel’dovich Ya.B., Raizer Yu.P., 2002, Physics of Shock Waves and High-Temperature Hydrodynamic Phenomena (New York: Dover)

APPENDIX A: A BRIEF REVIEW OF LAPLACE TRANSFORMS

We briefly review some of the relevant properties of Laplace Transforms. The Laplace transform, $f(s)$, of a function $F(t)$, where $t \geq 0$, is defined as

$$f(s) \equiv \mathcal{L}\{F(t)\} = \int_0^\infty \exp(-st) F(t) dt. \quad (\text{A1})$$

We will need the Laplace transforms of first and second derivatives of a function. Using (A1) these transforms can be related to the $f(s)$ by

$$\begin{aligned}\mathcal{L}\{F'(t)\} &= sf(s) - F(0) \\ \mathcal{L}\{F''(t)\} &= s^2 f(s) - sF(0) - F'(0),\end{aligned}\quad (\text{A2})$$

where the prime and double prime denote first and second order derivatives, respectively. The Bromwich integral expresses $F(t)$ in terms of $f(s)$ as

$$F(t) = \frac{1}{2\pi i} \int_{\gamma-i\infty}^{\gamma+i\infty} \exp(st) f(s) ds \quad (\text{A3})$$

where $i = \sqrt{-1}$ and γ is a real number chosen so that all poles of $f(s)$ lie, in the complex plane, to the left of the vertical line defining the integration path. Therefore, by the residue theorem we have

$$F(t) = \sum [\text{residues of } \exp(st) f(s)] \quad (\text{A4})$$

As an example consider $f(s) = 1/(s - s_1)(s - s_2)$ which has two simple poles at $s = s_1$ and s_2 . The residues of $\exp(st)f(s)$ at these poles are $\exp(s_1 t)/(s_1 - s_2)$ and $-\exp(s_2 t)/(s_1 - s_2)$ so that, by (A4), $F(t) = [\exp(s_1 t) - \exp(s_2 t)]/(s_1 - s_2)$. If $s_1 = s_2$, the function has a pole of order two at s_1 . The residue in this case is $d[(s - s_1)^2 \exp(st)f(s)]/ds$ evaluated at $s = s_1$. Therefore, $F(t) = t \exp(s_1 t)$.

APPENDIX B: STABILITY BY MEANS OF NYQUIST DIAGRAMS

Given a polynomial, P_N , of degree, N , Nyquist diagrams provide an easy and elegant method for determining the number of its roots which lie to the right of the imaginary axis, i.e., roots with a positive real part. The method can be summarized as follows: *a*) plot a contour of the value of the polynomial in the complex plane when its argument, s , is varied from $s = +i\infty$ to $s = -i\infty$ along the imaginary axis and *b*) use the contour diagram to compute the increase, $\Delta\psi$, in the phase of $P_N(s)$ as s moves along the imaginary axis. The number of roots with positive real parts is then $(\Delta\psi + N\pi)/(2\pi)$.

Figure (B1) shows Nyquist diagrams for the polynomial $B(s)$ given in (16) for three cases as indicated in the figure. In the top panel the phase changes from $-\pi/2$ to $-3\pi/2$ and therefore the number of roots with positive real parts is 1. Further, in this case this root has zero imaginary part since otherwise its conjugate is also be a root and there would be two roots with positive (and equal) real parts. In the middle panel the change is -3π and no roots lie to the right of the imaginary axis. In the bottom panel there are two roots with positive real parts.

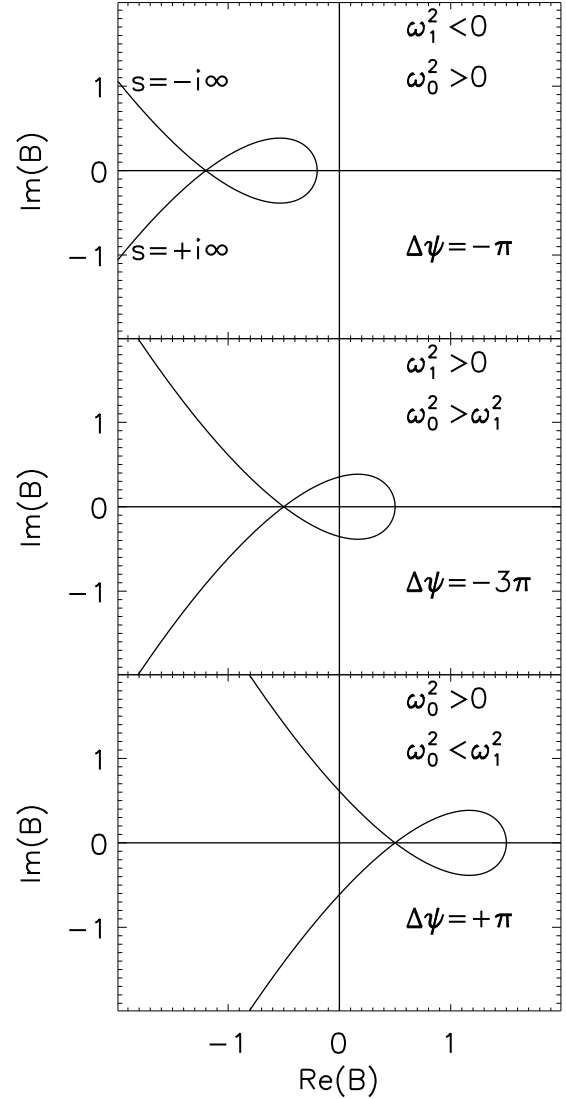


Figure B1. Nyquist diagrams of the polynomial $B(s)$.